A&A 439, 947–956 (2005)
DOI: 10.1051/0004-6361:20042395

Astronomy & Astrophysics

Extra-planar gas in the spiral galaxy NGC 4559⋆

C. V. Barbieri[1,4], F. Fraternali[2], T. Oosterloo[3], G. Bertin[4], R. Boomsma[5], and R. Sancisi[1,5]

[1] INAF – Osservatorio Astronomico, via Ranzani 1, 40127 Bologna, Italy
e-mail: claudia.barbieri@bo.astro.it
[2] Theoretical Physics, University of Oxford, 1 Keble Road, Oxford OX1 3NP, UK
[3] ASTRON, PO Box 2, 7990 AA, Dwingeloo, The Netherlands
[4] Università degli Studi di Milano, Dipartimento di Fisica, via Celoria 16, 20133 Milano, Italy
[5] Kapteyn Astronomical Institute, University of Groningen, The Netherlands

Received 19 November 2004 / Accepted 15 April 2005

Abstract. We present 21-cm line observations of the spiral galaxy NGC 4559, made with the Westerbork Synthesis Radio Telescope. We have used them to study the H I distribution and kinematics, the relative amount and distribution of luminous and dark matter in this galaxy and, in particular, the presence of extra-planar gas. Our data do reveal the presence of such a component, in the form of a thick disk, with a mass of 5.9×10^8 $M_\odot$ (one tenth of the total H I mass) and a mean rotation velocity 25−50 km s^{-1} lower than that of the thin disk. The extra-planar gas may be the result of galactic fountains but accretion from the IGM cannot be ruled out. With this study we confirm that lagging, thick H I layers are likely to be common in spiral galaxies.

Key words. galaxies: halos – galaxies: individual: NGC 4559 – galaxies: ISM – galaxies: kinematics and dynamics

1. Introduction

A large number of spiral galaxies have been observed in the 21-cm hydrogen line in recent years. Such observations serve two main purposes. One is to study the properties of the H I distribution and kinematics, and in particular the structure of the gaseous disk, the presence of extra-planar gas, the disk-halo connection, and the interactions with the environment. The other is to study the distribution of mass, the presence of dark matter, and its relationship with luminous matter.

Here we report 21-cm line observations of the spiral galaxy NGC 4559. The main result of these observations is the discovery of an extensive system of extra-planar gas in this galaxy.

Evidence for extra-planar gas in spiral galaxies is difficult to obtain and, to date, is available for only a few systems. The study of the edge-on galaxies NGC 891 (Swaters et al. 1997) and UGC 7321 (Matthews & Wood 2003) has revealed the presence of neutral gas up to several kiloparsecs from the plane and a lag in rotation with respect to the disk. A lagging H I layer has also been observed in NGC 2403, a galaxy viewed at intermediate inclination ($i \simeq 60°$) (Fraternali et al. 2002). Observations of face-on galaxies have shown vertical motions of neutral gas frequently associated with "holes" in the H I distribution (Puche et al. 1992; Kamphuis 1993; Boomsma et al. 2002). Vertical gradients in rotation velocity have also been found in the ionized gas (e.g. NGC 5775, Rand 2000).

These results suggest a complex gas circulation between disk and halo in spiral galaxies: ionized gas, swept up by stellar winds and supernova explosions, rises above the disk, cools down, and falls back to the plane. Such a *galactic fountain* (Shapiro & Field 1976) is not the only possible interpretation for the presence of gas outside the plane. Accretion of intergalactic "primordial" gas, as proposed for the High Velocity Clouds in our Galaxy (Oort 1970), or minor mergers with small companions (e.g. van der Hulst & Sancisi 1988) may also play an important role.

In the present study we use the 21-cm line observations of the spiral galaxy NGC 4559 to investigate the structure and the kinematics of the disk, the dark matter halo, and the presence of the extra-planar gas. The spiral galaxy NGC 4559 is an isolated Scd II galaxy at a distance of 9.7 Mpc (Tully 1988) and seen at an inclination angle of 67°. It has a radially extended H I layer (about 1.5 the optical size, $R_{25} = 15.82$ kpc) and regular kinematics (see Broeils 1992). Various studies of NGC 4559 have been carried out in X-ray both with ROSAT (Vogler et al. 1997) and with XMM and Chandra (Cropper et al. 2004). They have revealed the presence of diffuse X-ray emission and of some Ultra Luminous X-ray sources with luminosities $L_X \gtrsim 10^{40}$ erg s^{-1}, probably associated with regions of intense star formation (Soria et al. 2005).

In this paper, after a description of the H I observations of NGC 4559 in Sect. 2, we derive the rotation curve (Sect. 3). Then, in Sect. 4 we focus on the kinematically "anomalous" gas component and show that such gas forms a lagging thick

⋆ Figure 2 is only available in electronic form at http://www.edpsciences.org

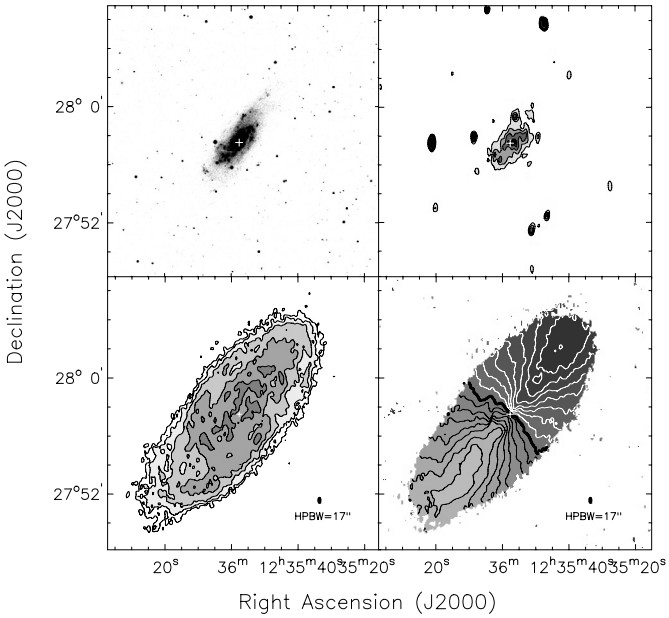

Fig. 1. *Top left panel*: optical image (DSS). *Top right panel*: radio continuum. The contour levels are 2, 3, 5, 6, 8, 10, 12, 14, 15σ, with σ = 0.15 mJy beam^{-1}. The column density contours in the total H I image (*bottom left*) are 1.5, 3, 6, 12, 24 × 10^{20} atoms cm^{-2}. *Bottom right panel*: velocity field at 17″ resolution. In the velocity field, contours are separated by 15 km s^{-1}; the thick line marks the systemic velocity (810 km s^{-1}). The receding side is darker. The scale factor is 1′ = 2.8 kpc. A small cross indicates the kinematical centre of the galaxy.

layer surrounding the cold H I disk. In Appendix A we present a mass model for NGC 4559, and briefly describe the properties of the dark halo.

2. Observations

The DSS (Digitized Sky Survey) image of NGC 4559 is presented in Fig. 1. The optical disk shows a multiple-armed spiral structure. The South-West side is the near side, assuming that the spiral arms are trailing. The main optical and radio parameters are summarized in Table 1. We have observed NGC 4559 with the Westerbork Synthesis Radio Telescope (WSRT). The WSRT observing parameters are summarized in Table 2.

2.1. Data reduction

Calibration and data reduction have been performed using the standard procedures of the MIRIAD (Multichannel Image Reconstruction, Image Analysis and Display) package. The MIRIAD task UVLIN has been used to derive the radio continuum emission and to subtract it from the line channels. This was done by interpolating with a straight line between the channels free of line emission at both ends of the band. Using all baselines we have obtained the full resolution (17″ = 790 pc) data cube. We have applied a Hanning smoothing to these data. The velocity resolution is 8.2 km s^{-1}. We have also produced data cubes at resolutions of 26″ and 60″. The raw images have been deconvolved with the CLEAN algorithm (Clark 1980).

Table 1. Optical and radio parameters for NGC 4559. (1) Tully (1988); (2) Karachentsev & Kopylov (1990); (3) Holmberg (1958); (4) Gavazzi & Boselli (1996); (5) 2MASS catalog; (6) RC2 catalog; (7) This work.

Parameter	NGC 4559	Ref.
Morphological type	Scd	4
Luminosity class	II	6
Optical centre		
(α, δ J2000)	$12^h35^m57\overset{s}{.}6$ +27°57′31.″4	2
Kinematical centre		
(α, δ J2000)	$12^h35^m58^s \pm 7^s$ +27°57′32″ ± 5″	7
Distance (Mpc)	9.7 (1′ = 2.8 kpc)	1
$L_B(L_\odot)$	1.06×10^{10}	4
$L_K(L_\odot)$	2.53×10^{10}	4
Disk scale length (kpc)	1.9	5
R_{25}(kpc)	15.82	1
$R_{\rm Ho}$(kpc)	16.24	3
Systemic velocity (km s^{-1})	810 ± 4	7
Mean H I inclination angle (deg)	67.2 ± 0.6	7
Mean position angle (deg)	−37.0 ± 1.4	7

Table 2. Observation parameters.

	NGC 4559
Observation date	2001 Feb. 01; June 29
Length of observation	2 × 12 h
Number of antennas	14
Baseline (min-max-incr)	36-m 2700-m 36-m
Pointing	
(α, δ J2000)	$12^h35^m57\overset{s}{.}7$ +27°57′35.″99
Central velocity (km s^{-1})	594.4
Central frequency (MHz)	1419.747
Total bandwidth (MHz)	2458
Total bandwidth (km s^{-1})	525
Number of channels	128
Channel separation (kHz)	19.2
Channel separation (km s^{-1})	4.1

A summary of the parameters for the three cubes is given in Table 3.

2.2. H I distribution and kinematics

We have analyzed the data cubes using the Groningen Image Processing System (GIPSY).

We have obtained total H I images at all three resolutions by adding the channel maps containing line emission (from 688.6 km s^{-1} to 957.2 km s^{-1}). In each channel map, we have defined the region of the H I emission by applying masks to the data. The masks have been obtained by smoothing the 26″ resolution data cube and applying a cutoff of 2σ. Figure 1 shows the total H I image and the velocity field

Table 3. Parameters of the data cubes.

	NGC 4559		
	17″	26″	60″
HPBW (″)	12.2×24.5	22.7×30.9	60.0×60.0
HPBW (kpc)	0.57×1.14	1.05×1.44	2.8×2.8
PA of synthesized beam (deg)	0.2	1.0	1.0
rms noise per channel (mJy beam^{-1})	0.52	0.48	0.68
rms noise per channel (K)	1	0.4	0.1
Minimum detectable column density (5σ):			
per resolution element (atoms cm^{-2})	7.73×10^{19}	3.0×10^{19}	0.83×10^{19}
per resolution element ($M_\odot$ pc^{-2})	0.63	0.24	0.06
Conversion factor (K mJy^{-1})	2	0.86	0.17

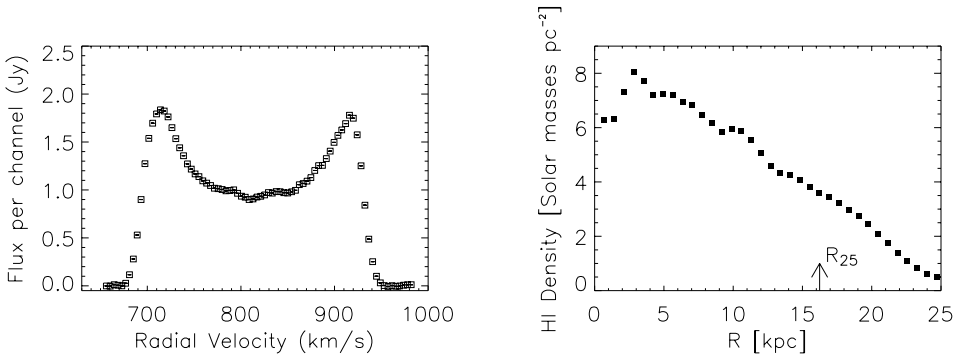

Fig. 3. Global H I line profile (*left*) and column density radial profile (*right*).

at 17″ resolution. This has been obtained by fitting, at each position, a Gaussian to the line profiles. Figure 2 gives the H I channel maps at 26″ resolution.

Figure 3 (left panel) shows the global H I line profile obtained by adding the flux densities for each channel map. The H I mass of NGC 4559, corrected for the primary beam attenuation, is $(6.75 \pm 0.02) \times 10^9$ $M_\odot$. This agrees with the value of 6.72×10^9 $M_\odot$ obtained by Broeils (1992) and of 6.4×10^9 $M_\odot$ derived by Shostak (1975) with the NRAO (National Radio Astronomical Observatory) 300-foot (91 m) telescope. The right panel of Fig. 3 shows the radial profile of the H I column density for NGC 4559 obtained by averaging the column densities in ellipses with position and inclination angles as reported in Table 1. Note the depression in the centre ($R < 2.5$ kpc) and the linear decline in the outer regions.

The H I density distribution and kinematics of NGC 4559 are not symmetric on the two sides of the galaxy. The lopsidedness in the density distribution can be seen in Fig. 1 (bottom left panel). The disk is more extended on the approaching side (S–E), reaching out to 26.6 kpc from the centre, while on the receding side it reaches 22.4 kpc. These are the distances, along the major axis, from the centre of the galaxy to the last column density contour of 0.6 $M_\odot$ pc^{-2}. The S–E part is warped (see channels from 685.1 km s^{-1} to 734.6 km s^{-1}). The warp is also visible in the total H I image and in the velocity field (Fig. 1). In Sect. 3 we derive separate rotation curves for the two halves of the galaxy and show that they differ significantly, i.e. the galaxy is lopsided also in its kinematics. This can be seen in the velocity field as a different shape of the iso-velocity contours in the northern and the southern sides. Despite these asymmetries in the H I distribution and kinematics, the global H I line profile shown in Fig. 3 is highly symmetric. This is a surprising result of the combined effects of lopsidedness in kinematics and in density distribution. In the past, studies of the occurrence of lopsidedness in spiral galaxies have been based on the shape of the global line profiles (Richter & Sancisi 1994; Haynes et al. 1998). The present result indicates that such studies are likely to have missed a significant fraction of galaxies that, like NGC 4559, are lopsided, despite the symmetry of their global line profiles.

The position-velocity (p–v) diagrams parallel to the major and to the minor axes (Figs. 5 and 8) show that the H I line profiles are asymmetric with respect to the peak. In Fig. 5 (left) the rotation curve (white dots) follows the ridge of the H I emission and broad, low-level extensions are visible toward the systemic velocity. At positions close to the galaxy centre (0′ to +2.′5), there are traces of emission at "forbidden" velocities (upper left quadrant) differing by about 150 km s^{-1} from the rotation velocity. This "forbidden H I" is also visible in the individual channel maps between 817 km s^{-1} and 874.7 km s^{-1}, southeast of the centre. The asymmetric line profiles appear similar to those observed in NGC 2403 (Fraternali et al. 2002). They suggest the existence of an H I component other than the thin, regularly rotating disk (cf. Fig. 5 left and right panels).

The H I distribution shows several holes. The most remarkable is located at $\alpha = 12^h36^m4^s$ $\delta = 27°57'7''$ (see Sect. 5.1).

3. Rotation curve

We have used the velocity field shown in Fig. 1 to obtain the kinematical parameters and the rotation curve of NGC 4559. For this we have followed the standard tilted-ring fitting procedure described by Begeman (1987). The rings have been chosen with a radial increment corresponding to the beamwidth of the observations (17″). Points have been weighted by the cosine of the azimuthal angle with respect to the major axis. To determine the position of the kinematical centre and the systemic velocity, only rings within 22.4 kpc from the galaxy centre have been considered. The mean values of the centre position and of the systemic velocity are reported in Table 1.

We have then proceeded to determine the inclination angle. In this procedure, the two sides of the galaxy are analyzed separately. The H I distributions on the two sides of the galaxy (see Sect. 2.2) are different. We have fitted the tilted rings out to 22.4 kpc on the receding side and out to 26.6 kpc on the approaching side. We have obtained mean values for the inclination angle in the approaching and receding sides by averaging such values between $R = 5$ kpc and $R = 17$ kpc. Outside this range the inclination angle is not constant. We found $i = 66.1° \pm 0.8°$ and $i = 68.4° \pm 0.6°$ for the approaching and receding sides respectively. Finally, we have determined the position angles separately for the two sides of the galaxy. The mean values (obtained by averaging over the whole galaxy) for the inclination and the position angles are $67.2° \pm 0.6°$ and $-37.0° \pm 1.4°$, respectively.

Using the values found for the inclination and position angles, we have determined the rotation curve first for the two sides of the galaxy separately and then for the whole galaxy (Fig. 4). As already noted, NGC 4559 is kinematically lopsided. The rotation curves of the two sides of the galaxy are significantly different. The rotation curve of the approaching side rises to 110 km s^{-1} inside 5 kpc and subsequently flattens, while on the receding side it continues to rise out to the outer parts where it reaches 123 km s^{-1}. This can also be seen in the velocity field, where the isovelocity contours are more curved on the approaching S–E side (see Fig. 1).

In the Appendix we present two mass models for NGC 4559. The maximum disk fit gives a mass-to-light ratio $M/L = 0.27$ in K-band. In order to determine the error bars of the rotation curve in Figs. 7 and A.1, we have constructed a residual velocity field by subtracting a model from the observed velocity field. Then, we have taken the mean values along ellipses defined by the position and the inclination angles obtained from the tilted-ring model analysis. In this way the error bars give also a measure of the deviations from circular motion.

4. Extra-planar gas

The H I position-velocity diagram along the major axis (Fig. 5, left panel) shows the presence of systematic asymmetries in the form of wings in the line profiles away from the rotation velocity (white dots) and towards the systemic velocity. The model

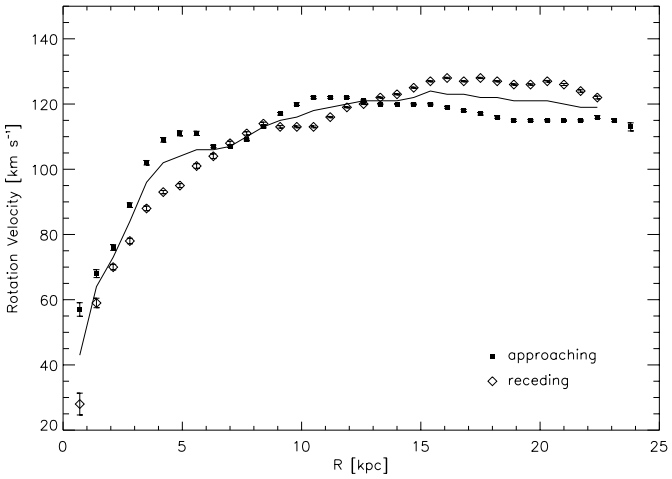

Fig. 4. Rotation curves obtained for the two sides of NGC 4559. The continuous line shows the curve obtained for the whole galaxy.

of a thin H I disk with a Gaussian velocity profile (cold disk), as shown in the right hand panel of the same figure, does not have such wings. We call the gas responsible for these wings "anomalous" gas. The presence of anomalous gas is more striking in the approaching than in the receding part of the galaxy; such a difference is probably related to the kinematic lopsidedness of the cold disk (see Sect. 5.2). A similar anomalous gas component was found in NGC 2403 (Fraternali et al. 2002) and was interpreted as an extra-planar component that forms a thick H I layer embedding the thin disk. Most likely the two components do not coexist in the region close to the equatorial plane.

4.1. Distribution and kinematics of the anomalous H I

In order to study the distribution and kinematics of the anomalous H I, we have separated it from the regular H I component. We have assumed that the thin cold disk contribution to the line profile is described by a Gaussian function centered on the rotation velocity of the galaxy and we have defined as "anomalous gas" the H I emission not included in the Gaussian profile. The cold disk has thus been modeled by fitting a Gaussian function to the line profile, after applying a clip to the data at the level of 10% of the peak value. The obtained velocity dispersions are in the range 8−12 km s^{-1}. The resulting Gaussian model cube has been subtracted from the data, generating a new cube made only of the residual anomalous gas. This has all been done with the 17″ data cube. Subsequentely, the residual cube has been smoothed to 60″ resolution to improve the *S/N* ratio.

The left panel of Fig. 6 shows the distribution of the anomalous gas overlaid on the optical image. Its diameter is 43 kpc and the total mass is about 5.9×10^8 $M_\odot$ (that is, about 1/10 of the total H I mass). The velocity dispersion of this anomalous gas, obtained from the 3D models discussed below (see Sect. 4.2), is about 12−25 km s^{-1}. The right panel of the same figure presents the intensity-weighted mean velocity field of the anomalous gas. Much like for the cold disk, the kinematics of the anomalous gas is dominated by differential rotation.

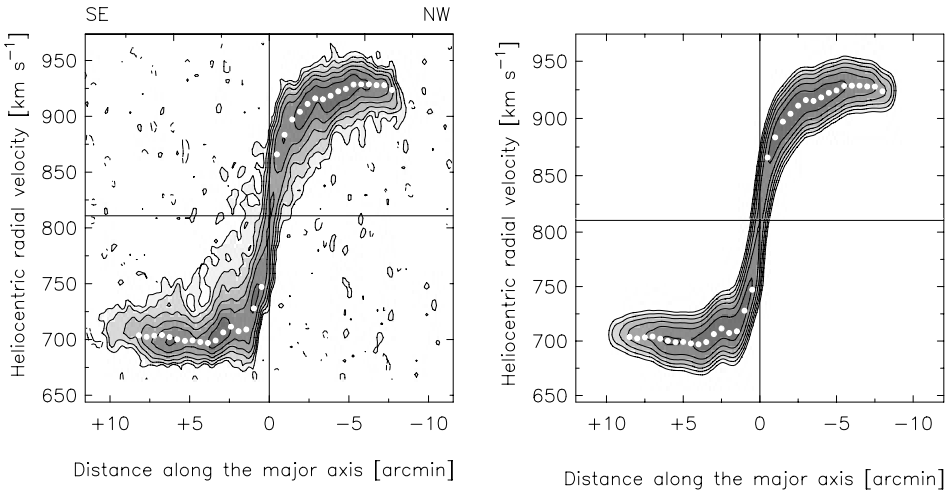

Fig. 5. *Left*: H I p–v diagram at 26″ resolution along the major axis of NGC 4559 (PA = −37°, V_{sys} = 810 km s^{-1}). *Right*: model p–v diagram along the major axis for a thin H I disk. Contours are −2, 2, 4, 8, 16, 32, 64σ, with σ = 0.48 mJy beam^{-1}. The white dots show the (projected) rotation curve.

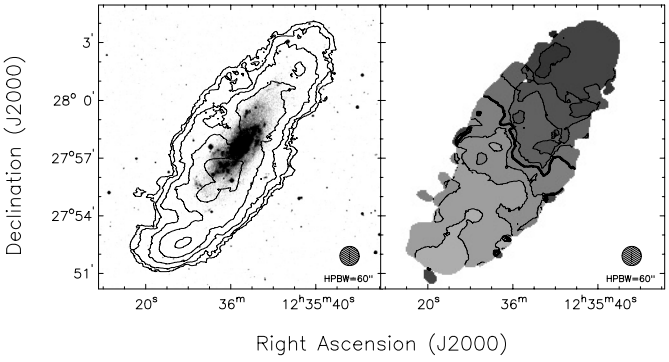

Fig. 6. Total H I image (*left*) and intensity-weighted mean velocity field (*right*) for the anomalous gas in NGC 4559. The column density contours are 1, 2, 4, 8, 16, 32 × 10^{19} atoms cm^{-2}. *The left panel* shows the density distribution of the anomalous gas overlaid on the optical DSS image of the galaxy. The right panel shows the velocity field, with isovelocity contours separated by 25 km s^{-1}; the thick line corresponds to the systemic velocity.

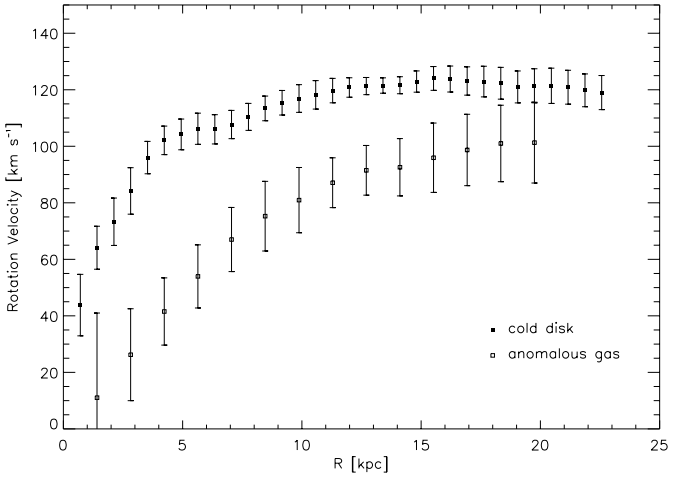

Fig. 7. Rotation curves for the cold disk (filled symbols, same as in Figs. 4 and A.1, 17″ data), and for the anomalous gas (open symbols). The curve for the anomalous gas has been obtained from the 60″ data.

The spatial distribution of the anomalous gas is quite homogenous and isotropic (but see Sect. 5.2). This is only partially due to the low resolution of the image in Fig. 6 and suggests that the anomalous gas is not the result of a single recent local event (such as the capture of a lump of gas) but instead of a widely spread phenomenon. Moreover, the kinematics of the anomalous gas is regular and closely follows that of the thin disk. This suggests a close relation with the thin disk, as in a galactic fountain (see Sect. 5.3).

We have fitted the tilted ring model to the velocity field of the anomalous gas in order to obtain the rotation curve. This has been done by setting all the relevant geometrical parameters fixed to the values found for the cold disk. The uncertainties in the derivation of the rotational velocities (error bars in Fig. 7) have been estimated from the residual velocity field, by taking the mean values along ellipses as done for the cold disk (see Sect. 3). Figure 7 shows the rotation curves of the cold disk and of the anomalous gas. The difference is of about 20 km s^{-1} in the outer regions and 60 km s^{-1} in the inner parts. Table 4 summarizes the properties of the cold disk and of the anomalous gas.

4.2. Models

First of all we have to understand if the anomalous gas has a truly anomalous kinematics or if the anomalies that are found are produced by projection effects due to the inclination and/or thickness of the H I disk. We have done this with the aid of 3D models made with the task GALMOD (GIPSY) modified by us to include radial motions and a vertical density profile for the thick disk. We have considered several variations of a two-component structure, made of a thin and a thicker, but lower density layer. These two components do not actually coexist in

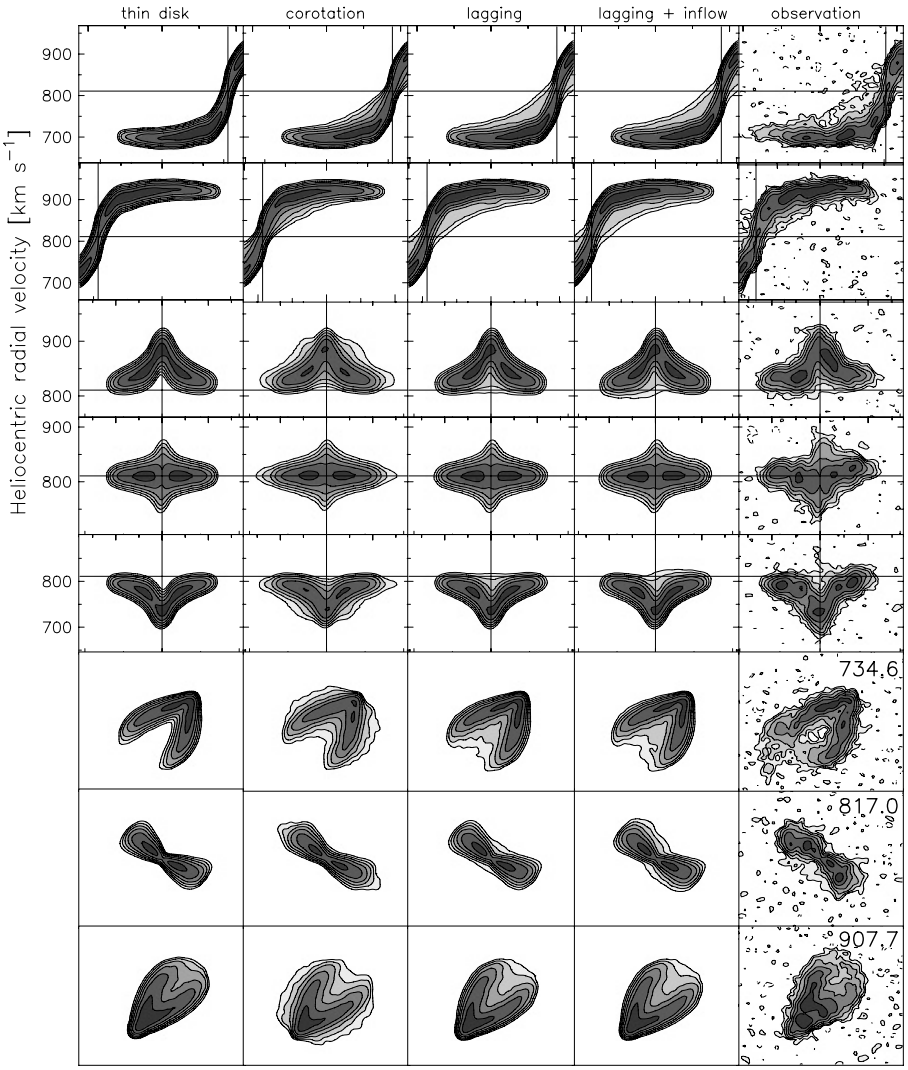

Fig. 8. Comparison of the H I observations of NGC 4559 with different models. The rightmost column shows the data at 26″ resolution. *From the top*: position-velocity along the major axis on the approaching side and on the receding side, parallel to the minor axis (+1′ N–W, minor axis, −1′ S–E) and three channel maps (the heliocentric radial velocities are on the top right of the data frames). Contours are −2, 2, 4, 8, 16, 32, 64σ, with σ = 0.48 mJy beam^{-1}. *From the left*: one-component model made of a thin (scale height = 0.2 kpc) disk (thin disk); two-component model made of a thin disk and a co-rotating thicker (scale height 4 kpc) layer (corotation); two-component model made of a thin disk and a slowly rotating thicker (scale height 2 kpc) layer (lagging) and with a radial motion toward the centre of the galaxy (lagging + inflow).

the same spatial region of the equatorial plane. The input values for the rotation curve and the radial H I density profile are those derived from the data. The models have been inspected in the same way as the data cube to make a full comparison with the data. Figure 8 shows the position-velocity diagrams along the major axis (upper two rows), three cuts along and parallel to the minor axis (central three rows), and three channel maps (lower three rows). The observations are in the rightmost column. The leftmost column shows the thin disk model (scale height 0.2 kpc). The scale height of the thin disk used here is similar to that of the neutral hydrogen layer of the Milky Way or of other galaxies seen edge-on. Note, however, that the size of the regions that can be resolved in the data is a factor ≥5 times larger than the adopted scale height for the thin disk. Clearly, the thin disk model fails to reproduce the tail at low rotation velocities in the observed p–v diagram along the major axis.

Table 4. Properties of the cold disk and of the anomalous gas.

Parameter	Cold disk	Anomalous gas
Mass ($M_\odot$)	6.2×10^9	5.9×10^8
Total extent (kpc)	49	43
Scale height (kpc)	0.2	≤4 [1]
Maximum rotation velocity (km s^{-1})	123	102
Mean velocity dispersion (km s^{-1})	8–12 [2]	12–25 [2]

[1,2] Values obtained from the 3D model. [2] The mean velocity dispersion ranges from the lower value in the outer parts to the upper value in the inner parts of the galaxy.

We have tried to reproduce this tail by varying only the thickness of the gas layer. To this end, we have constructed a two-component structure (second column) made of a thin

disk (scale height 0.2 kpc) and a corotating thicker layer (scale height 4 kpc). This model does reproduce part of the low level emission visible in the position-velocity diagram along the major axis, but the $p-v$ diagrams parallel to the minor axis and the channel maps disagree with the data. This shows that the anomalous gas in NGC 4559 cannot be caused by thickness effects alone. The third column shows a model in which the gas layer is composed of two non-corotating components: a thin disk (scale height 0.2 kpc) rotating with the rotation curve found for the cold disk (Fig. 7) and a thick disk (scale height 2 kpc) rotating with the rotation curve of the anomalous gas shown in Fig. 7. This model provides a good representation of the data showing that the anomalous gas is indeed produced by a combination of lagging and thickness.

The velocity field of the anomalous gas (Fig. 6) shows that the projected kinematical minor axis (thick line) differs, mainly in the inner part, from that of the cold disk (cf. Fig. 1). In NGC 2403 the projected kinematical minor axis appears to be rotated with respect to that of the cold disk. This has been explained in terms of an overall inflow motion of the extra-planar gas towards the centre of the galaxy (Fraternali et al. 2002). We have explored the possibility of an inflow motion of the anomalous gas toward the centre also for NGC 4559, by making a model (column next to the data) equal to the previous one with the addition of a radial motion toward the galaxy centre (inflow) of 15 km s^{-1}. There are some hints of radial motion also in NGC 4559, but the evidence is not as strong as for NGC 2403.

5. Discussion and conclusions

5.1. Holes in the H I distribution

The H I distribution shows several holes. One of the most remarkable is located at $\alpha = 12^{\rm h}36^{\rm m}4^{\rm s}$ $\delta = 27°57'7''$, a location marked by a small white ellipse in Fig. 9. The hole has a diameter of about 1 kpc. It is especially clear in the position-velocity diagrams parallel to the minor and to the major axis, centered on the hole, shown in Fig. 9. In the direction of the hole, we see a broadening and splitting of the line profile. This is the signature of an expanding shell of gas moving away from the disk into the halo. The systemic radial velocity of the shell is 760 km s^{-1}. If we assume an isotropic expansion, the expansion velocity of the spherical shell is about 30 km s^{-1} as measured along the line of sight. However, the expansion of the shell might be anisotropic and faster in the direction perpendicular to the disk, toward the low-density halo. In this case, we would be observing the projected component of the expansion velocity which could then be as large as 80 km s^{-1}.

The hole is not completely empty, but contains a mass of about 3×10^6 $M_\odot$. From the surrounding regions, we have estimated an average column density of 2.5×10^{21} cm^{-2}, that would be expected if no hole were present. The mass required to fill the hole is then $\sim 2 \times 10^7$ $M_\odot$. This mass is comparable to the sum of the mass of gas moving away from the disk ($\simeq 5 \times 10^6$ $M_\odot$) and the mass of the part of the shell presumably moving tangentially ($\simeq 7 \times 10^6$ $M_\odot$). The hole and the shell may have been produced by supernova explosions or stellar winds. An estimate of the kinetic energy of the swept up gas gives values between 2×10^{53} erg and 1×10^{54} erg.

If the expansion of the H I shell is isotropic, the kinematic age of the hole lies between 6×10^6 yr and 1.5×10^7 yr. If the hole was initially spherical, the differential rotation of the galaxy may be the cause of the observed elongation of the hole in the direction of rotation. The time necessary to produce such a stretching is of the order of 10^7 yr. Another way to estimate the age of the hole is to use the velocity dispersion ($\sim$10 km s^{-1}) of the gas surrounding the hole. One may expect the hole to be filled in 5×10^7 yr.

If holes and bubbles are produced by supernova explosions or stellar winds, there should be some correlation with star formation in the disk. Moreover the bubbles might be filled with hot gas (a few 10^6 K) which should be visible in the X-rays (Norman & Ikeuchi 1989). However, from an analysis of ROSAT observations of NGC 4559, Vogler et al. (1997) did not find any excess X-ray emission in the region of the hole. Therefore, there is no evidence for the existence of hot gas in the H I hole. If the kinetic energy is of the order of a few 10^{53} erg, a hundred to a thousand supernovae would be required to produce the hole. We note that the hole is located within the optical disk where the star formation activity is high. A type II supernova explosion was observed in NGC 4559 in 1941 (SN 1941, Kowal & Sargent 1971), at $\alpha = 12^{\rm h}35^{\rm m}55.5^{\rm s}$ $\delta = 27°58'0''$ (see the small white dot in Fig. 9), far away from the hole.

5.2. Extra-planar gas and the lopsidedness of NGC 4559

High sensitivity observations of NGC 4559 have revealed the presence of "anomalous" gas rotating more slowly than the gas in the disk. 3D models have shown that this anomalous gas is indeed a slowly rotating extra-planar component. In Sects. 2 and 3 we have shown that the gaseous disk of NGC 4559 is lopsided both in density distribution and in kinematics. Here we investigate the possible lopsidedness of the extraplanar gas by constructing separate models for the approaching and receding sides of the galaxy.

Figure 10 shows the observed position-velocity diagram along the major axis on the approaching and the receding sides (rightmost column). The extra-planar gas component appears to be more pronounced on the approaching side of the galaxy. This may simply mean that the less steep rotation of the receding part of the galaxy conspires to partly hide the anomalous gas on that side. The first column of Fig. 10 shows the model position-velocity diagrams for the two parts of the galaxy, with a thin disk (scale height 0.2 kpc) and a more slowly rotating thicker layer (scale height 2 kpc). The rotation curves and the radial H I density profiles used for the thin disk are those derived separately for the approaching and for the receding sides, whereas the thicker layer is kept symmetrical. The observed asymmetry is reproduced, but not completely. On the approaching side, the model reproduces less anomalous gas than observed, while on the receding side it seems to produce slightly more. A somewhat better reproduction of the asymmetry can

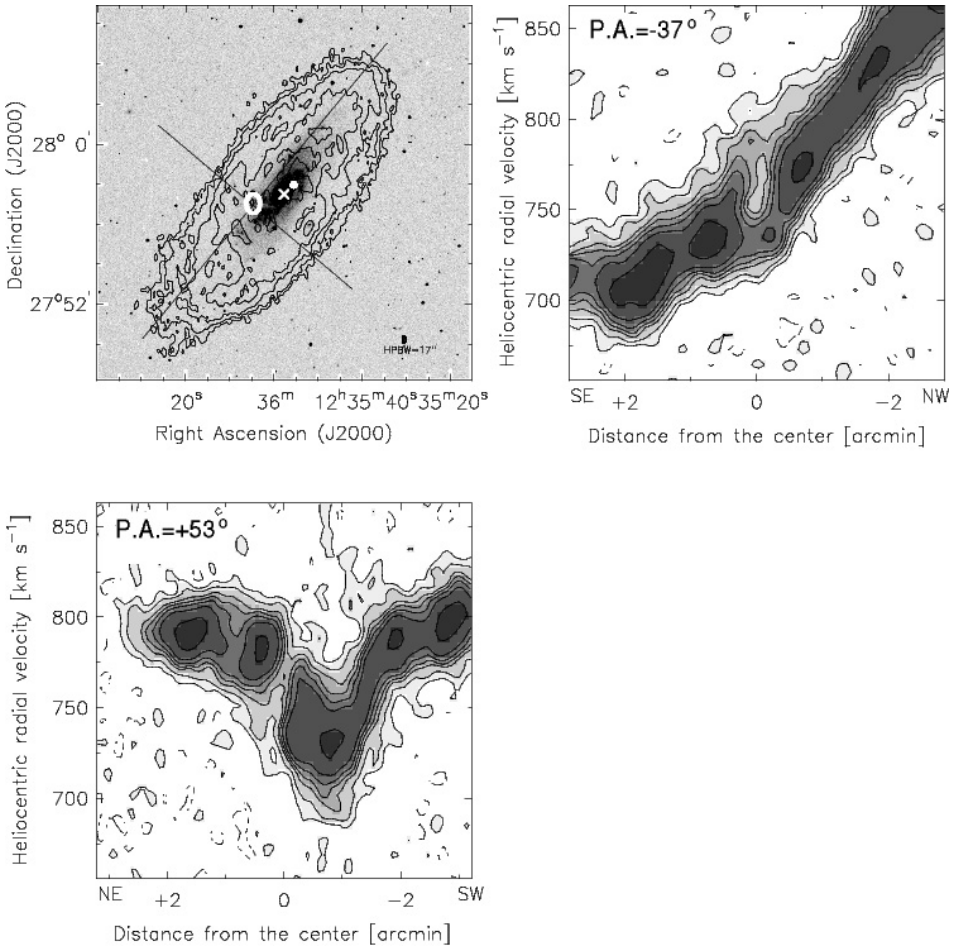

Fig. 9. *Top left*: total H I column density distribution superposed on the optical image (DSS). The H I contours range from 1.5×10^{20} to 2.4×10^{21} atoms cm^{-2}. The cross marks the position of the centre of the galaxy and the white dot indicates the position of SN 1941. The cuts are parallel to the major and the minor axis and centered on the H I hole (white ellipse). Shown are also the corresponding position – velocity map (17″ resolution) parallel to the major axis (*top right*) and to the minor axis (*bottom left*). The contour levels are −1.5, 1.5, 3, 6, 8, 11, 16, 32σ, with σ = 0.52 mJy beam^{-1}. Negative contours are dashed.

be obtained in two different ways. The first is to consider different rotation curves of the extra-planar gas on the two sides of the galaxy, lower on the approaching and higher on the receding side. The second is to make the thick disk thicker on the approaching and thinner on the receding side. In model b of Fig. 10 we have done this. We show here a model composed of a thin disk (scale height 0.2 kpc) and a more slowly rotating thicker layer. For the thin disk we have used the same input values of the previous model whereas we have made the thick disk more massive and thicker on the approaching side (scale height 3 kpc against 1 kpc). This model provides a good representation of the data. Here, the rotation curve of the thick layer has been kept symmetrical. If, however, the H I layer on the approaching side is indeed thicker, its rotation velocity may be lower as found for NGC 891 by Fraternali et al. (2004).

In conclusion, it seems that the density distribution and the kinematics of the extraplanar gas in NGC 4559 are not azimuthally symmetric. The extraplanar gas seems more abundant on the approaching side. In the optical and radio continuum images (Fig. 1), this side appears brighter than the receding one and possibly has, therefore, higher star formation activity (see also the X-ray image in Cropper et al. 2004). Moreover, this is the side where the rotation curve rises more steeply indicating a higher concentration of mass. The fact that the extraplanar gas seems prominent on this side supports the idea of a link between extraplanar gas and star formation.

Another indication of the connection with star formation comes from the presence of the forbidden gas, i.e. the gas seen in Figs. 5 and 10 near the centre (0′ to +2.′5, upper left quadrant) at "forbidden" velocities differing by about 150 km s^{-1} from the rotation velocity. This gas is not reproduced by our model probably because we have not considered vertical motions. It is interesting to note that the forbidden component is found only in the central regions (within 5 kpc) of the galaxy and mainly on the approaching side. Moreover, this region is close to the remarkable hole in the H I distribution described in Sect. 5.1.

5.3. The origin of the extra-planar gas

The origin of the extra-planar gas is not known. The main question is whether it is caused by processes that take place in the galactic disk or whether it originates from infall of extragalactic, primordial gas.

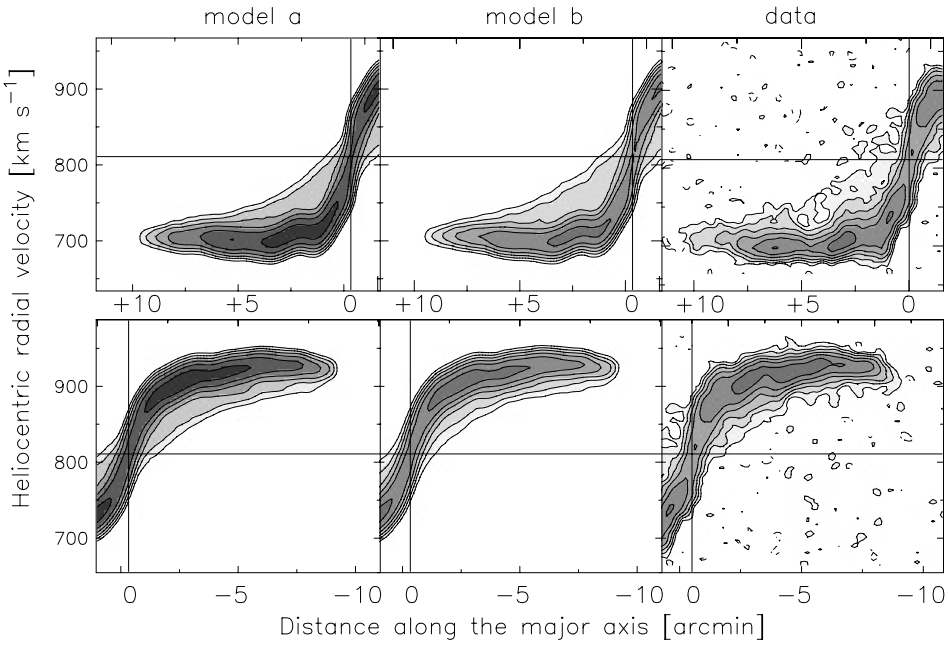

Fig. 10. Comparison of the H I observations of NGC 4559 with different models. Position-velocity map along the major axis for the approaching side (*top*) and for the receding side (*bottom*). The rightmost column shows the data at 26″ resolution. Contours are −2, 2, 4, 8, 16, 32, 64σ, with σ = 0.48 mJy beam^{-1}. First column: two-component model made of a thin disk (scale height 0.2 kpc) and a slowly rotating thicker (scale height 2 kpc) layer (model a). Second column: two-component model made of a thin disk (scale height 0.2 kpc) and a slowly rotating layer with a scale height of 3 kpc on the approaching side and of 1 kpc on the receding side (model b).

With this study we have collected new evidence for a close relation between the extra-planar gas and the star formation activity: 1) the overall kinematical pattern of the extraplanar gas is regular and suggests a close connection with the underlying thin disk of NGC 4559 and a galactic fountain origin; 2) the extraplanar gas seems more abundant on the brighter (approaching) side of the galaxy; 3) there is evidence for fast moving gas complexes (forbidden gas) and large expanding HI supershells. Moreover; 4) the extra-planar gas appears to be regularly distributed over the whole galaxy. This suggests that the extraplanar gas is unlikely to be due to a local phenomenon, such as the recent accretion of a massive cloud, and it is more likely to be the result of a widely spread activity such as star formation. Indeed, observations in other bands provide evidence for a regularly distributed star formation activity in the disk of NGC 4559 (e.g. Cropper et al. 2004).

However, despite all these arguments apparently favoring an internal origin of the extra-planar gas, an interpretation of the observed phenomena in terms of accretion from the intergalactic medium cannot be ruled out completely. In fact, the above arguments, which do suggest a link between the extraplanar gas and star formation in the disk, could be reversed to conclude that the higher star formation rate might be the end result of accretion rather than the cause at the origin of extraplanar gas.

It is also worth mentioning here that, using X-ray and HST optical data, Soria et al. (2005) claim to have found evidence for a recent collision of a satellite dwarf with the disk of NGC 4559.

In conclusion, the strongest point in favor of an internal origin seems to be the kinematical pattern of the extra-planar gas. It is very difficult to produce such a regular pattern from accretion of external material having, in principle, randomly oriented angular momentum. This suggests that at least a significant fraction of the extra-planar gas is likely to originate from galactic fountains.

The extra-planar gas of NGC 4559 is similar to that found by Swaters et al. (1997) in the edge-on spiral galaxy NGC 891, by Matthews & Wood (2003) in UGC 7321, and by Fraternali et al. (2002) in NGC 2403. The parameters for the thick disk derived in these studies are similar. For instance, the extraplanar gas in NGC 2403 has a mass of 1/10 of the total H I mass, a mean rotation velocity of 25−50 km s^{-1} lower than that of the disk, and a radial inflow of about 10−20 km s^{-1} towards the galaxy centre. The H I observations presented here are, together with those of NGC 2403, NGC 891 and UGC 7321, among the deepest ever obtained. This suggests that the extra-planar gas may be a common feature in spiral galaxies, missed earlier because of insufficient sensitivity of the previous observations. Clearly, new observations are required to confirm this interesting possibility and to study the relations of the extra-planar gas with the galaxy morphological type, star formation rate, and environment.

Acknowledgements. Claudia Barbieri is grateful to ASTRON (Dwingeloo), to the Kapteyn Astronomical Institute (Groningen), to the INAF-Osservatorio Astronomico di Bologna and to the Istituto di Radioastronomia (CNR, Bologna) for their hospitality and financial support. The Westerbork Synthesis Radio Telescope is operated by the ASTRON (Netherlands Foundation for Research in Astronomy) with support from the Netherlands Foundation for Scientific Research NWO.

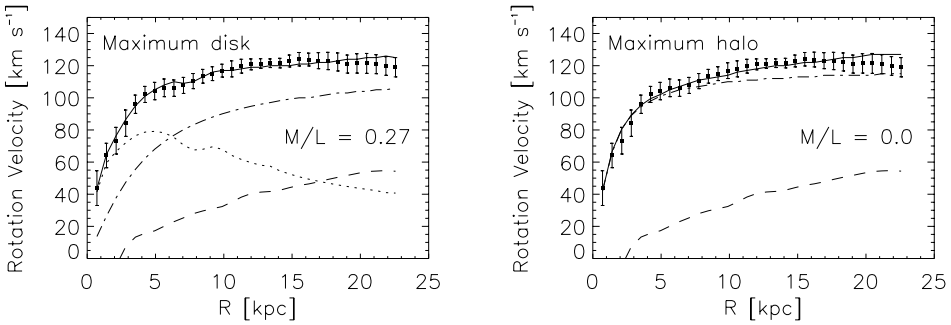

Fig. A.1. Two different mass models for NGC 4559. The filled squares show the observed rotation curve. The contributions of the gas (dashed), stars (short dashed) and dark matter halo (long-short dashed) are shown. The values of the mass-to-light ratio are for the K band.

Appendix A: mass model

The rotation curve shown in Fig. 4 serves as the basis for the study of the galaxy dynamics. The adopted mass model consists of three components (Begeman 1989): the stellar disk, the gas disk, and the dark matter halo. For the stellar component we have used the surface brightness profile in K-band obtained from the 2MASS catalog (Jarrett et al. 2003), fitted with an exponential law for radii larger than 0.8 kpc. The derived scale length is 1.9 kpc and the central brightness is 17.14 mag/arcsec^2. Figure 3 (right panel) shows the radial column density profile for the neutral hydrogen. This has been obtained from the observed total H I map, using the kinematical parameters from the tilted ring model. The gas column density is obtained by multiplying the H I density by a factor 1.4 to take into account the helium content. Note that NGC 4559 shows a central depression in the hydrogen distribution ($R \leq 2$ kpc). Since the force field is calculated from the observed H I surface density, the potential of the gaseous disk may be such that for the innermost regions there is a net outward pull, resulting formally in imaginary rotation velocities. For this reason, the velocity contribution of the gaseous disk in Fig. A.1 starts from a radius of about 2 kpc. For the scale heights, we have assumed a value of 0.4 kpc for the stellar and 0.2 kpc for the gas layer. The velocity contribution of the luminous disk (star + gas) has been obtained from the formula given by Casertano (1983). For the dark matter halo we have adopted a spherically symmetric density profile $\rho(R) = \rho_0(1 + R/R_0)^{-2}$, where ρ_0 is the central density and R_0 is the core radius.

Figure A.1 shows two different fits to the rotation curve. The maximum-disk solution is presented in the left panel. The corresponding value of the mass-to-light ratio, obtained using the photometric profile in K band, is 0.27 $M_\odot/L_{K,\odot}$. This value includes the contribution of the molecular gas component, based on the assumption that this follows the light distribution (Young & Knezek 1989). The second model is the so-called maximum halo, in which formally no stellar disk is considered (0.0 $M_\odot/L_{K,\odot}$). The quality of the fits are comparable. Analyzing the sample of Ursa Major galaxies, Verheijen (1997) finds that the K' mass-to-light ratios of the High Surface Brightness galaxies under the maximum disk hypothesis typically range from 0.4 to 1.0, slightly higher than the value found here.

References

Begeman, K. G. 1987, Ph.D. Thesis, University of Groningen
Begeman, K. G. 1989, A&A, 223, 47
Boomsma, R., Oosterloo, T., Sancisi, R., & van der Hulst, J. M. 2002, BAAS, 34, 708
Broeils, A. H. 1992, Ph.D. Thesis, University of Groningen
Casertano, S. 1983, MNRAS, 203, 735
Clark, B. G. 1980, A&A, 89, 377
Cropper, M., Soria, R., Mushotzky, R. F., et al. 2004, MNRAS, 349, 39
Fraternali, F., van Moorsel, G., Sancisi, R., & Oosterloo, T. 2002, AJ, 123, 3124
Fraternali, F., Oosterloo, T., Sancisi, R., & Swaters, R. A. 2004, Proceedings Workshop, Extra-planar gas, Dwingeloo, June 2004, ed. R. Braun
Gavazzi, G., & Boselli, A. 1996, ApL&C, 35, 1
Haynes, M. P., van Zee, L., Hogg, D. E., Roberts, M. S., & Maddalena, R. J. 1998, AJ, 115, 62
Holmberg, E. 1958, Lund Medd. Obs. Ser. II, No. 136
Jarrett, T. H., Chester, T., Cutri, R., Schneider, S., & Huchra, J. P. 2003, AJ, 125, 525
Kamphuis, J. J. 1993, Ph.D. Thesis, University of Groningen
Karachentsev, I. D., & Kopylov, A. I. 1990, MNRAS, 243, 390
Kowal, C. T., & Sargent, W. L. W. 1971, AJ, 76, 756
Matthews, L. D., & Wood, K. 2003, ApJ, 593, 721
Norman, C. A., & Ikeuchi, S. 1989, ApJ, 345, 372
Oort, J. H. 1970, A&A, 7, 381
Puche, D., Westpfahl, D., Brinks, E., & Roy, J.-R. 1992, AJ, 103, 1841
Rand, R. J. 2000, ApJ, 537, L13
Richter, O.-G., & Sancisi, R. 1994, A&A, 290, L9
Shapiro, P. R., & Field, G. B. 1976, ApJ, 205, 762
Shostak, G. S. 1975, ApJ, 198, 527
Soria, R., Cropper, M., Pakull, M., Mushotzky, R., & Wu, K. 2005, MNRAS, 356, 12
Swaters, R. A., Sancisi, R., & van der Hulst, J. M. 1997, ApJ, 491, 140
Tully, R. B. 1988, Nearby Galaxies Catalog (Cambridge: Cambridge University Press)
van der Hulst, T., & Sancisi, R. 1988, AJ, 95, 1354
Verheijen, M. A. W. 1997, Ph.D. Thesis, University of Groningen
Vogler, A., Pietsch, W., & Bertoldi, F. 1997, A&A, 318, 768
Young, J. S., & Knezek, P. M. 1989, ApJ, 347, 55

Online Material

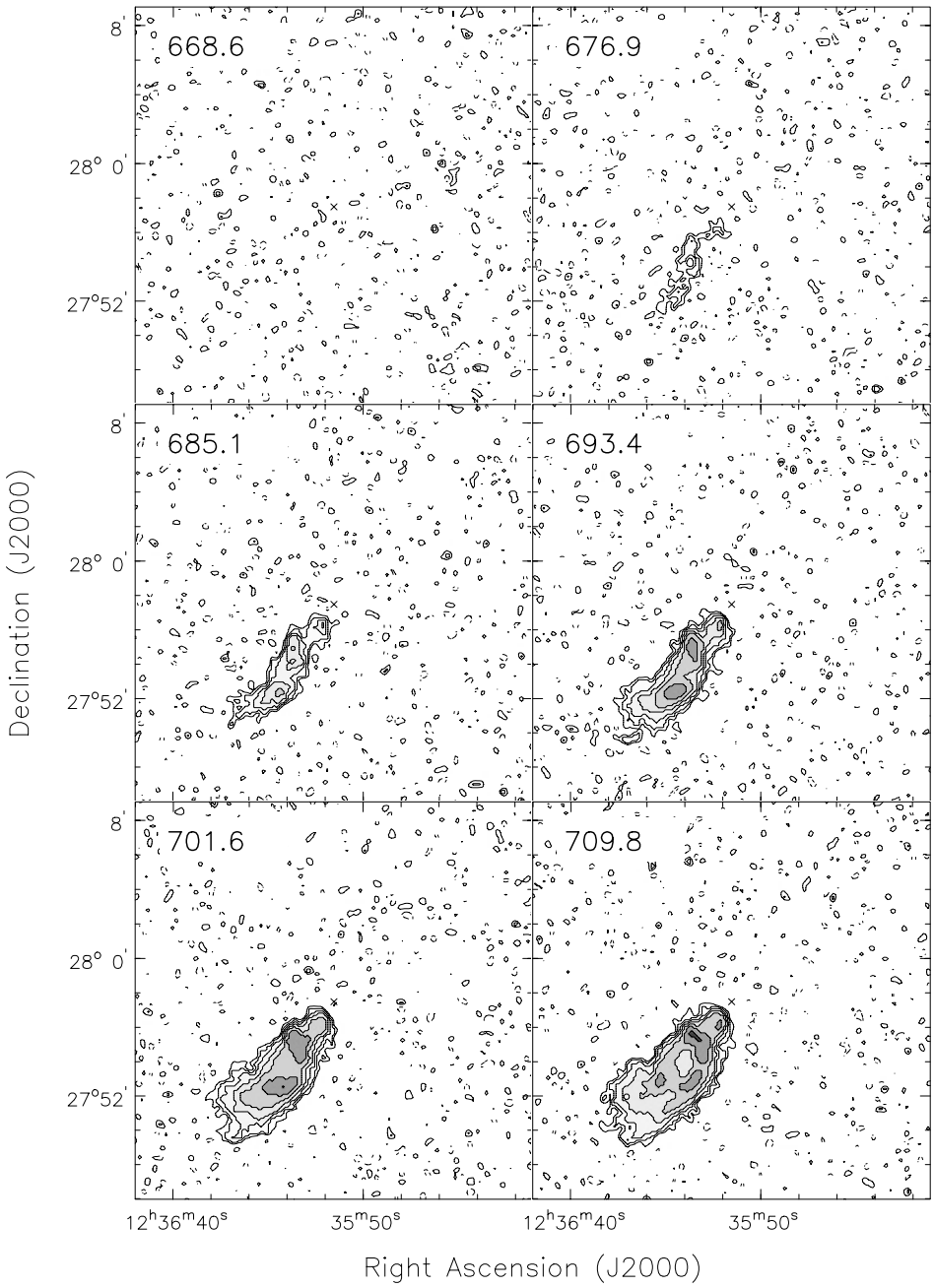

Fig. 2. H I channel map at 26″ resolution. The heliocentric radial velocity (km s^{-1}) is shown in the upper left corner. Contours are −2, 2, 4, 8, 16, 32, 64σ, with σ = 0.48 mJy beam^{-1}. A small cross indicates the kinematical centre of the galaxy.

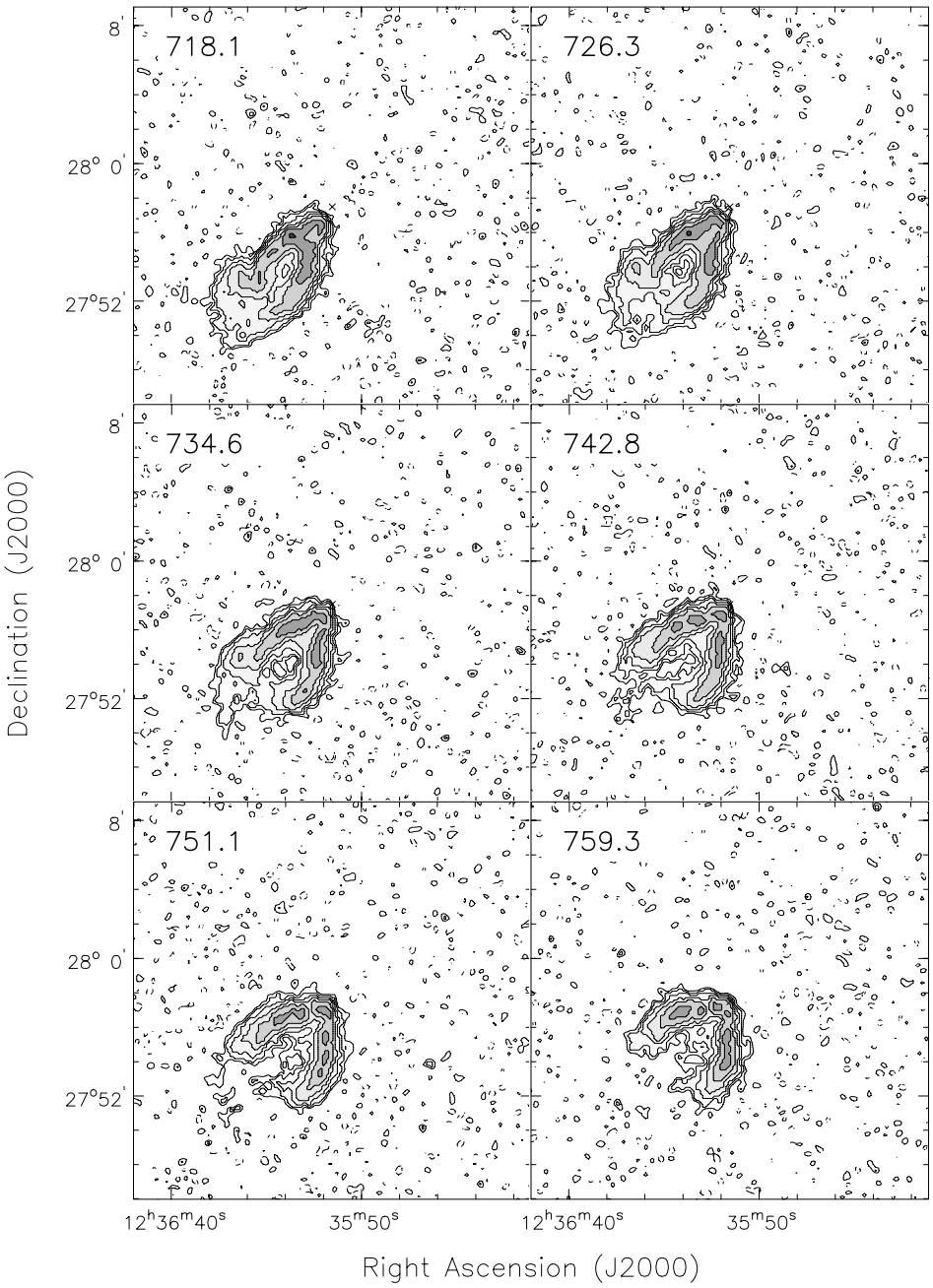

Fig. 2. continued.

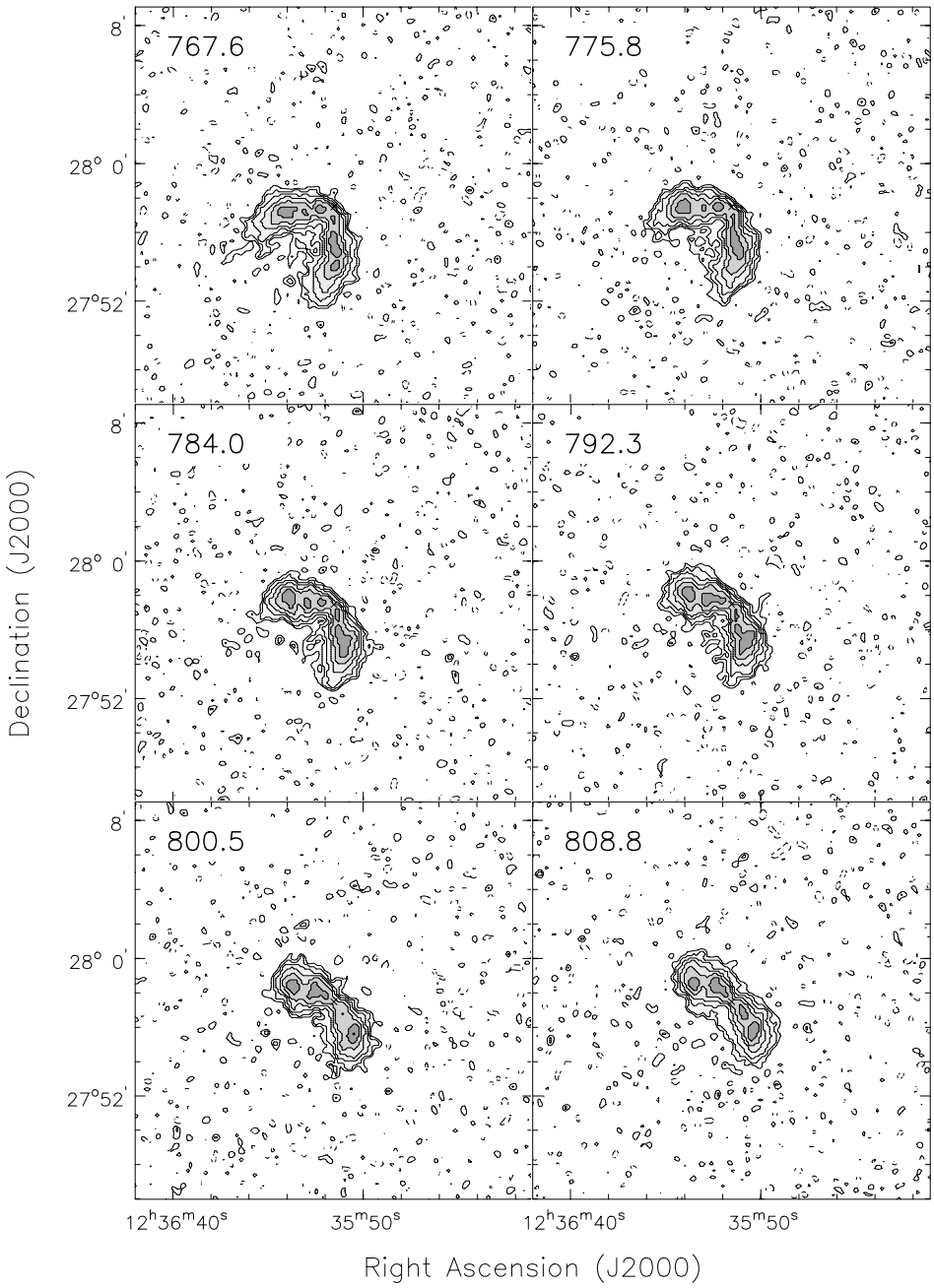

Fig. 2. continued.

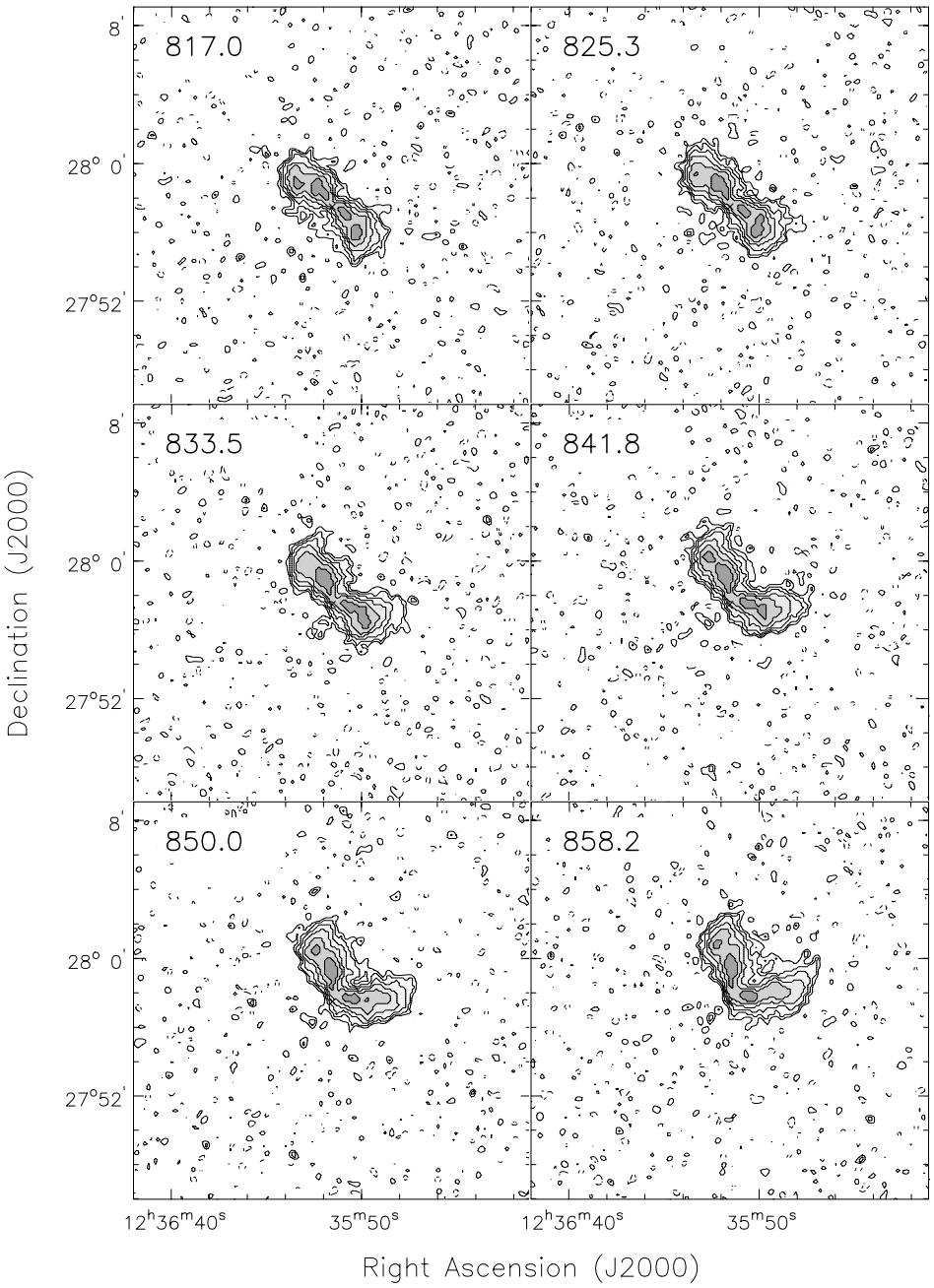

Fig. 2. continued.

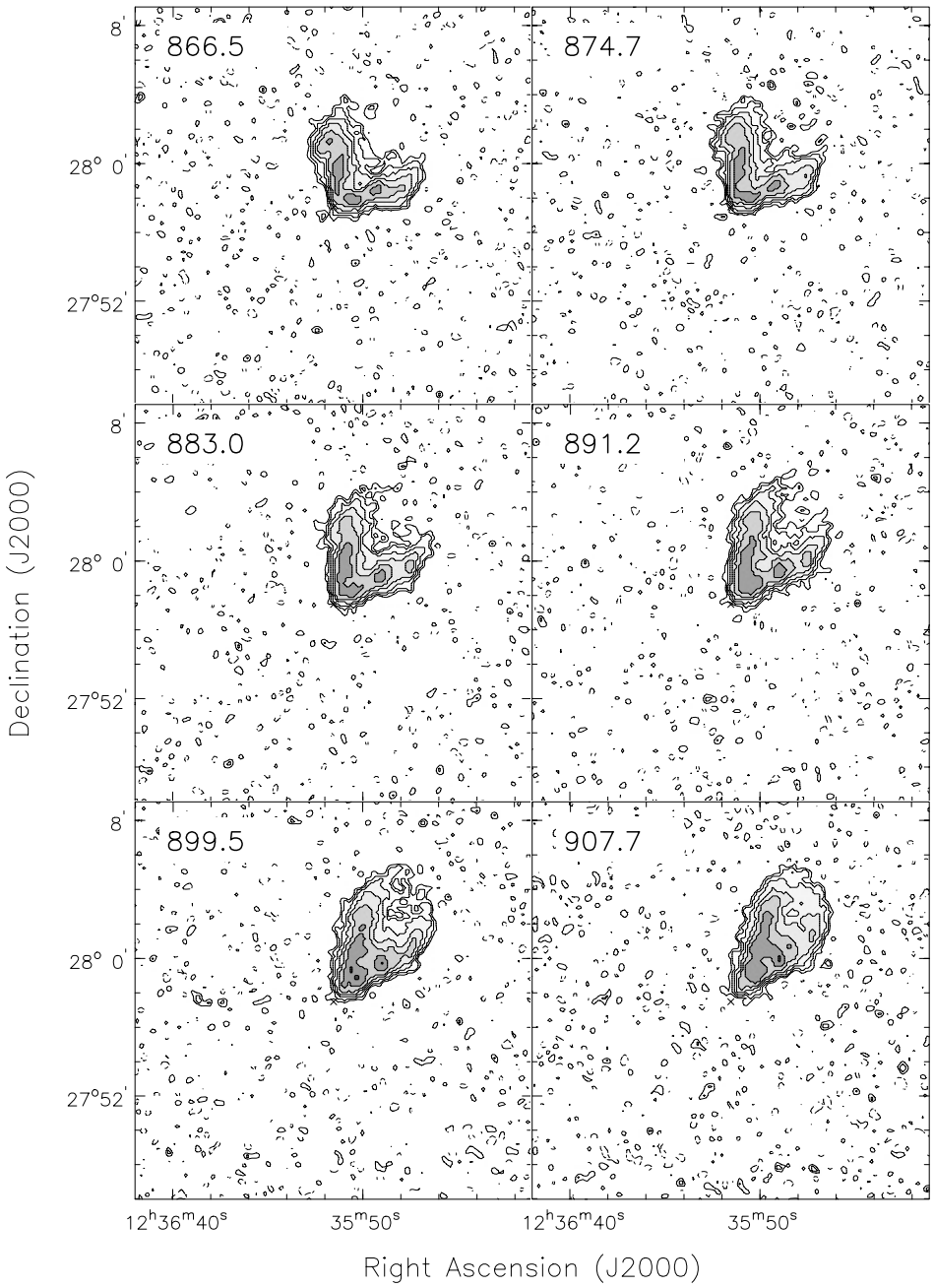

Fig. 2. continued.

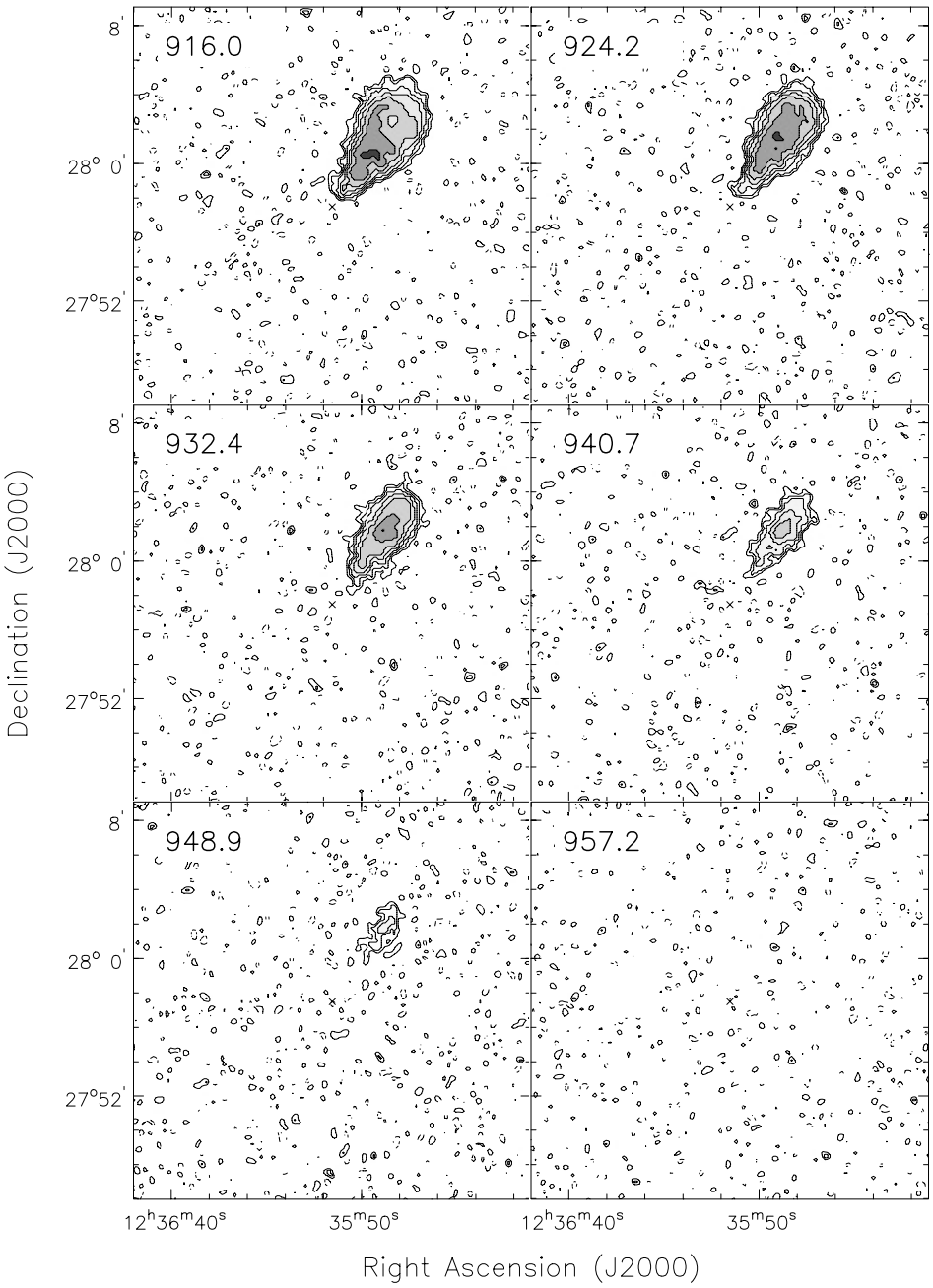

Fig. 2. continued.